

Observation of high-order moiré effect and multiple Dirac fermions replicas in graphene-SiC heterostructures

Chunlong Wu,^{1,*} Qiang Wan,^{1,*} Cao Peng,^{1,*} Shangkun Mo,¹ Renzhe Li,¹ Keming Zhao,¹ Yanping Guo,² Da Huo,² Chendong Zhang,² and Nan Xu^{1,†}

¹*Institute of Advanced Studies, Wuhan University, Wuhan 430072, China*

²*School of Physics and Technology, Wuhan University, Wuhan 430072, China*



(Received 22 June 2021; revised 17 November 2021; accepted 29 November 2021; published 16 December 2021)

Moiré potential has become a powerful tool to modulate electronic structures and realize quantum phases. Authors of previous studies mainly focused on the first-order moiré effect in systems with small lattice mismatches and rotation angles. Here, we report evidence of a high-order moiré effect and multiple Dirac cone replicas by performing angle-resolved photoemission spectroscopy on a graphene-SiC heterostructure. Despite that the first-order moiré effect is weak due to large lattice mismatch and rotation angle, a high-order moiré effect with a 1.9 nm periodicity in real-space is experimentally observed. Different from previously studied first-order moiré systems, in which only replicas with momentum transfer by the primitive reciprocal lattice vectors were observed, Dirac cone replicas with momentum transfer by second- and third-order reciprocal lattice vectors are experimentally identified. Our results not only demonstrate the high-order moiré effect in a graphene-SiC heterostructure but also provide opportunities to engineer moiré systems without the limitation of small lattice constant mismatches.

DOI: [10.1103/PhysRevB.104.235130](https://doi.org/10.1103/PhysRevB.104.235130)

I. INTRODUCTION

Designing Dirac cone structures of graphene by moiré heterostructures has become a promising platform for realizations of quantum phases and phase transitions [1–36]. In the graphene-boron nitride (BN) heterostructure, the moiré potential generates clones of Dirac cones near the corners of the Brillouin zone (BZ) of graphene, which leads to a fractal energy spectrum in a strong magnetic field [1–7]. Recently, the moiré potential in twisted bilayer graphene [8,9] generated nearly flat bands with a strong electronic correlation, in which correlated insulators, superconductivity, and exotic quantum phases were achieved [10–24]. By introducing an additional superlattice potential from BN or WSe₂ into the twisted bilayer graphene and trilayer graphene, superconductivity, ferromagnetism, and the quantum anomalous Hall effect are realized [25–36].

Authors of previous studies mainly focused on the first-order moiré effect in systems with both small lattice mismatches [$\Delta a = (a_1 - a_2)$] and small twist angles (θ), as described in Fig. 1(a). In this case, the moiré lattice constant in real space is

$$a_m = \frac{1}{\sqrt{\left(\frac{1}{a_1}\right)^2 + \left(\frac{1}{a_2}\right)^2 - \frac{2\cos\theta}{a_1 a_2}}}. \quad (1)$$

In momentum space (k space), the corresponding moiré vector \vec{G}_m equals the difference between the primitive reciprocal lattice vectors of the component layers ($\vec{G}_1 - \vec{G}_2$)

in Fig. 1(b). Graphene-BN, twisted bilayer graphene, and twisted transition metal dichalcogenides [37] belong to this case, in which the first-order moiré effect dominates the systems.

Here, we experimentally identify a high-order moiré effect in a heterostructure with large Δa and θ and reveal the moiré modulation effect on an electronic structure by performing angle-resolved photoemission spectroscopy (ARPES) on graphene-SiC. The first-order moiré effect is weak in graphene-SiC, with a small moiré period of $a_m \sim 0.49$ nm according to the formula in Eq. (1). In contrast, the high-order moiré effect associated with the lattice mismatch $\Delta a'$ and twist angle θ' between the graphene- (2×2) supercell and the SiC- $(\sqrt{3} \times \sqrt{3})$ supercell is experimentally observed with $a'_m \sim 1.9$ nm. Different from the first-order moiré effect in graphene-BN and twisted bilayer graphene, in which only the Dirac cone replicas with momentum transfer by the primitive reciprocal lattice vector of the other consisting layer (first-order momentum transfer) are experimentally observed, we reveal additional multiple Dirac cone replicas stemming from the high-order moiré effect with momentum transfer by second- and third-order reciprocal lattice vectors of SiC (second- and third-order momentum transfers). Our results not only uncover a moiré system with multiple Dirac cones cloned by high-order moiré effects but also extend the application conditions of the moiré effect to heterostructures with large lattice constant mismatch.

II. EXPERIMENTAL DETAILS

ARPES measurements were performed at the home-designed facility with a base pressure better than 5×10^{-11} Torr and photon energy $h\nu = 21.2$ eV, at a

*These authors contributed equally to this work.

†nxu@whu.edu.cn

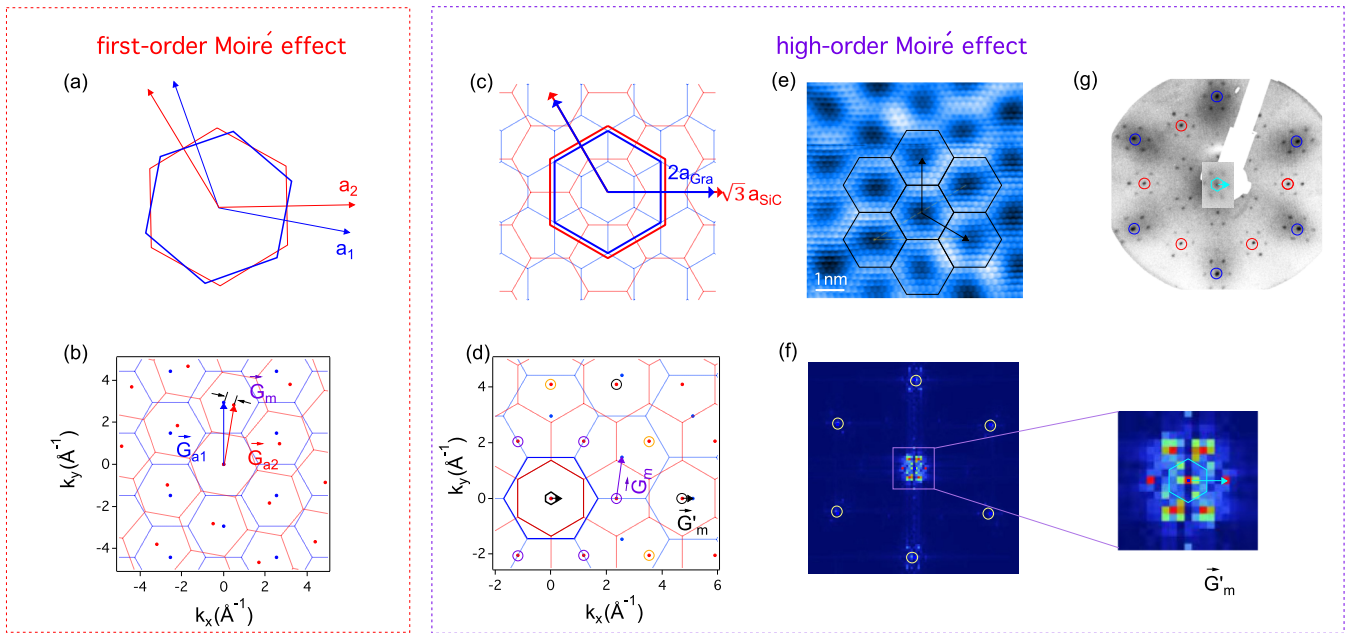


FIG. 1. (a) and (b) Schematic first-order moiré effect in real and k spaces, respectively. (c) and (d) Same as (a) and (b) but for the high-order moiré effect. The graphene (2×2) and SiC $\sqrt{3} \times \sqrt{3}$ supercells are marked by bold hexagons in (c). The moiré vector \vec{G}'_m in k space is labeled in (d). (e) Scanning tunneling microscope (STM) image of the graphene-SiC heterostructure. The moiré superstructure is labeled. (f) The corresponding fast Fourier transform (FFT) results. The arrow and hexagon in the zoomed-in area are the \vec{G}'_m vector and corresponding moiré Brillouin zone (BZ). (g) Low-energy electron diffraction (LEED) image of the graphene-SiC heterostructure. The blue and red circles mark the graphene and SiC structures, respectively. The area marked by the dashed rectangle, which is blocked by the electron gun in the normal emission geometry, is measured by rotating the sample off the normal emission.

temperature < 6 K. Low-energy electron diffraction (LEED) patterns were measured on the same sample surface using electron energy of 150 eV, with a facility mounted on the ARPES chamber. Scanning tunneling microscope (STM) measurements were performed by a commercial Unisoku 1300 system at 4.2 K with a constant current mode. Electrochemically etched tungsten tips were used in our measurements. Samples were directly transferred into the ARPES and STM chambers without breaking the vacuum. High-quality monolayer graphene was achieved by an annealing process [38] of n -type 6H-SiC(0001) from PrMat. Large-scale STM measurements confirmed that sample surfaces were covered by monolayer graphene in hundreds of nanometers, with small parts covered by bilayer graphene and SiC substrate. The band splitting as the signature of bilayer graphene was not observed in ARPES measurements due to the small fraction.

III. RESULTS

Compared with the first-order moiré effect in Fig. 1(a), both Δa and $\theta = 30^\circ$ are large in the graphene-SiC heterostructure [Fig. 1(c)]. The first-order moiré effect is expected to be weak with a small a_m in real space according to the formula in Eq. (1) and a large \vec{G}_m in k space [Fig. 1(d)]. On the other hand, we can construct a (2×2) supercell for graphene and a ($\sqrt{3} \times \sqrt{3}$) supercell for SiC, indicated by bold blue and red hexagons in Fig. 1(c),

respectively. Between these supercells, the lattice mismatch $\Delta a' = (\sqrt{3}a_{\text{SiC}} - 2a_{\text{Gra}})$ is quite small, and the twist angle $\theta' = \theta - 30^\circ = 0^\circ$, which is like the first-order moiré systems depicted in Fig. 1(a). Therefore, the high-order moiré effect related to $\Delta a'$ and θ' between the supercells is expected to be pronounced, with a moiré period $a'_m = \frac{a_{\text{Gra}} a_{\text{SiC}}}{\Delta a'} = 1.9$ nm according to the formula in Eq. (1).

The corresponding high-order moiré vector \vec{G}'_m in k space is the difference between the second reciprocal lattice vector of graphene and the third reciprocal lattice vector of SiC in Fig. 1(d). The high-order moiré vector \vec{G}'_m has a 0.38 \AA^{-1} length, which is much smaller than the first-order moiré vector \vec{G}_m . The \vec{G}'_m vector has the same orientation with the primitive vector of SiC, and 30° rotated from that of graphene.

The high-order moiré effect on electronic structure modulation in real space is suggested in the large-scale atom arrangement plot in Fig. S1 in the Supplemental Material [39] and directly observed by STM measurement in Fig. 1(e). We append a'_m vectors and the moiré superstructure, which fit the STM results very well. A fast Fourier transform (FFT) of STM data is shown in Fig. 1(f). Except the pattern labeled by gray circles corresponding to the original graphene structure, additional patterns related to a bigger superstructure are directly observed at the center and near the graphene pattern. As seen from a zoomed-in area of Fig. 1(f), the experimentally determined superstructure wave vector in k space fully agrees with the high-order moiré vector \vec{G}'_m in Fig. 1(d). The LEED pattern in Fig. 1(g) shows consistent signatures of \vec{G}'_m vectors

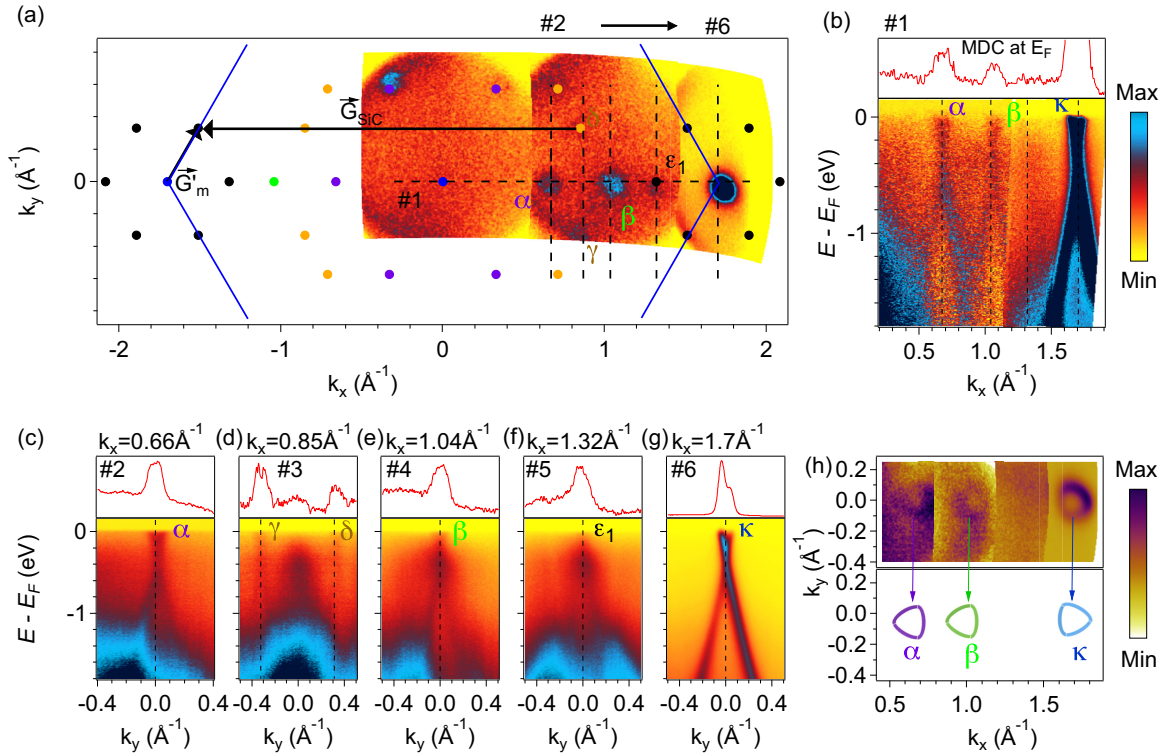


FIG. 2. (a) Fermi surface mapping of the graphene-SiC heterostructure. All the expected replicas are marked based on symmetries. (b)–(g) Photoemission intensity plots along the cut #1–6 in (a). The momentum distribution curves at E_F are appended on top. (h) Constant energy map at 1 eV below E_F . The triangle shapes are drawn for guiding of eyes.

near the center for graphene and SiC patterns. The LEED pattern corresponding to the SiC substrate also appears [red circles in Fig. 1(h)] because of a slightly deeper penetration depth of low-energy electrons than the tunneling current in STM measurements.

The high-order moiré effect on electronic structure modulation in k space is directly observed in ARPES measurements. In addition to the original Dirac cone at the K point of graphene, additional ARPES intensity hotspots clearly appear in the Fermi surface (FS) map shown in Fig. 2(a). The band dispersions cutting through these hotspots are Dirac conelike [Figs. 2(b)–2(f)], like the Dirac cone at the K point in Fig. 2(g). The locations of Dirac cone replicas are determined by the momentum distribution curves at E_F shown in Figs. 2(b)–2(g). In addition to the ε_1 band, there are more Dirac cone replicas (ε_2 – ε_6) forming a hexagonal shape centered at the K point, which have stronger spectra weight in the ARPES experiment using higher energy photons, as seen from Fig. S2 in the Supplemental Material [39]. We notice that each ε_i replica can be connected to one of the γ/δ bands by the \vec{G}_{SiC} vector, as seen from Fig. 2(a). This suggests that the interlayer coupling between graphene and the SiC substrate could play an important role in cloning the Dirac cones, as expected from the high-order moiré effect. Furthermore, as seen from Fig. 2(h), the constant energy plot at $E_B = 1$ eV indicates triangle-like shapes of the α and β replicas and the original cone. The α and β replicas show the different orientation to the original cone.

The experimentally observed Dirac cone replicas are fully explained by the high-order moiré effect with momentum

transfer. As seen from Fig. 3(a), the first-order momentum transfer shifts a pair of Dirac cones by the primitive vector of SiC (labeled by purple circles). The replicas are expected at the end points of the $\vec{K}_{m1}^{(1)}$ and $\vec{K}_{m2}^{(1)}$ vectors in Fig. 3(a), if putting the starting points of $\vec{K}_{m1}^{(1)}$ and $\vec{K}_{m2}^{(1)}$ vectors at the BZ center. We directly compare the $\vec{K}_{m1}^{(1)}$ and $\vec{K}_{m2}^{(1)}$ vectors with the symmetrized FS map determined by ARPES experiments in Fig. 3(b), which fit the α and β replicas very well. It also naturally explains the orientation of α and β replicas at $E_B = 1$ eV, shown in Fig. 2(h). As seen from Fig. 2(b), the α and β replicas corresponding to the $\vec{K}_{m1}^{(1)}$ and $\vec{K}_{m2}^{(1)}$ vectors have opposite valley properties. Therefore, the α and β replicas on the same side have the same valley property but opposite to the original Dirac cone at the K point [Fig. 3(b)].

In the first-order moiré-effect-dominated systems, for example, graphene-BN and twisted bilayer graphene heterostructures, only replicas with first-order momentum transfer are experimentally observed. In the graphene-BN system, the Dirac cone replicas form a hexagon centered at each K point, which is 30° rotated compared with the BZ of graphene [7]. In the graphene-SiC heterostructure with the high-order moiré effect, the Dirac cone replicas with first-order momentum transfer sit relatively far from the K point. They form two hexagons centered at the Γ point in the same orientation as the BZ of graphene. Furthermore, replicas with second- and third-order momentum transfers are also clearly observed in the graphene-SiC heterostructure. As seen from Fig. 3(a), the second-order momentum transfer process shifts a pair of Dirac cones marked by yellow triangles by the second primitive

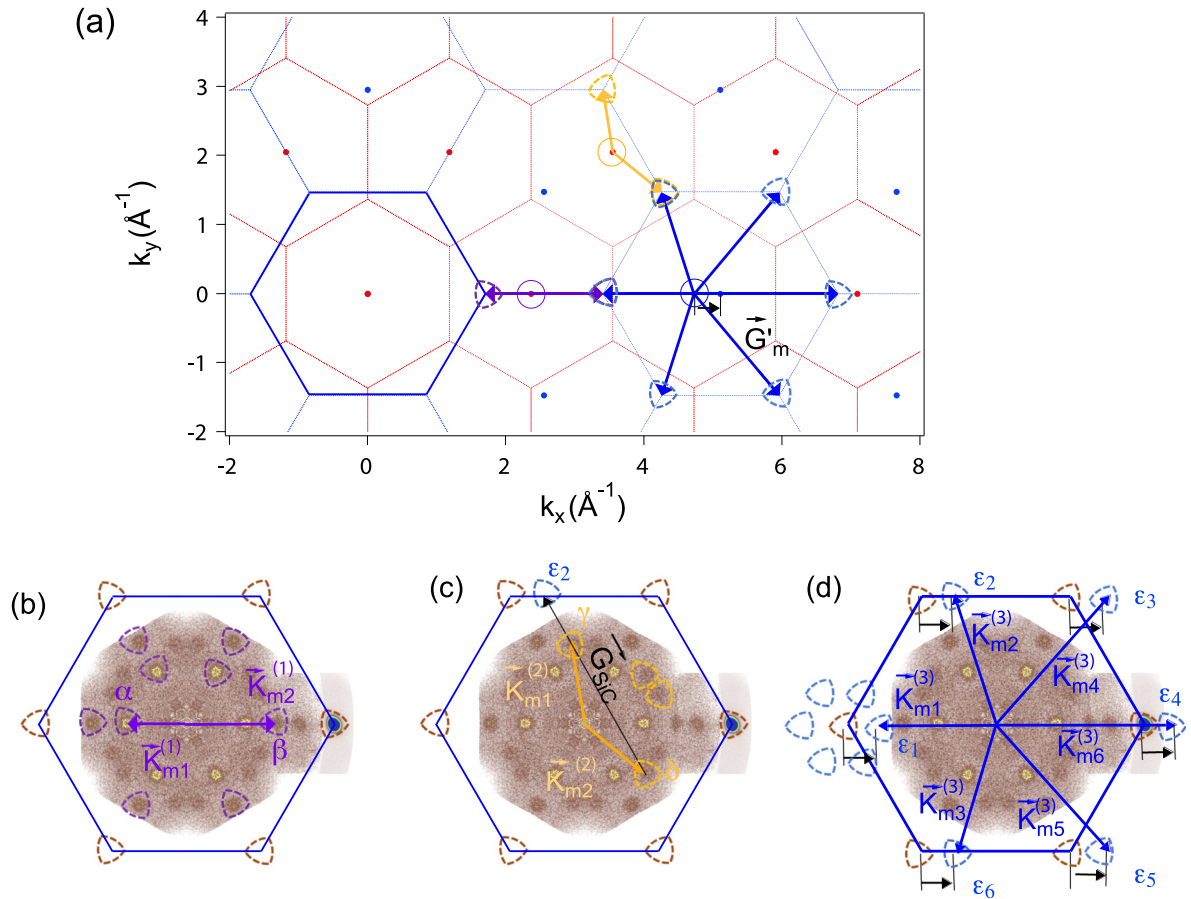


FIG. 3. (a) The schematic first-, second-, and third-order momentum transfer in the graphene-SiC heterostructure. (b) The direct comparison of the first-order momentum transfer vectors $\vec{K}_m^{(1)}$ and experimentally determined Dirac cone replicas. (c) and (d) Same as (b) but for the second-order momentum transfer vectors $\vec{K}_m^{(2)}$ and third-order momentum transfer vectors $\vec{K}_m^{(3)}$, respectively.

vectors of SiC (yellow circle). The locations of the ending points of $\vec{K}_{m1}^{(2)}$ and $\vec{K}_{m2}^{(2)}$ (yellow arrows) match the γ and δ replicas very well. The Dirac cone replicas with second-order momentum transfer form a pair of hexagons with $\pm 21.2^\circ$ rotated from the BZ of graphene.

Similarly, the third-order momentum transfer shifts the nearest six Dirac cones (blue triangles) by the third-order reciprocal lattice vectors of SiC (blue circle), as shown in Fig. 3(a). The locations of the ending points of $\vec{K}_{m1}^{(3)} - \vec{K}_{m6}^{(3)}$ (blue arrows) are fully consistent with the $\varepsilon_1 - \varepsilon_6$ replicas observed in Fig. 3(d) and Fig. S2 in the Supplemental Material [39]. As seen from Fig. 3(d), the wave vectors between the $\varepsilon_1 - \varepsilon_6$ Dirac cone replicas and the original Dirac cone at the K point are fixed. Compared with Fig. 3(a), such a wave vector equals the moiré vector \vec{G}'_m . This relationship forces $\varepsilon_1 - \varepsilon_6$ replicas to form a hexagon centered at each K point, which is fully consistent with the ARPES results with higher photon energy in the Supplemental Material [39] as well as previous results [40]. This structure of replicas is quite similar to the first-order momentum-transfer-induced ones in the graphene-BN system [7], but the orientation of \vec{G}'_m here is 30° rotated from \vec{G}_m in the graphene-BN system. Similar high-order momentum transfer processes were reported in the 30° twisted bilayer graphene system [41,42].

The momentum transfer vectors of the high-order moiré effect in Fig. 3(a) not only fit the experimentally observed Dirac cone replicas very well but also explain the relative geometry of the replicas. As seen from Figs. 3(a) and 3(c), the δ and ε_2 replicas originate from the same Dirac cone, shifted by the second- and third-order reciprocal lattice vectors of SiC, respectively. Therefore, the distance between the δ and ε_2 replicas equals the primitive vectors of SiC in Fig. 3(c). Similarly, the distance between the β and ε_1 replicas on the opposite side is also a primitive vector of SiC.

The observed Dirac cone replicas cannot be fully explained by the 6×6 [43] or $6\sqrt{3} \times 6\sqrt{3}$ [44,45] reconstructions. As illustrated in Fig. S3 in the Supplemental Material [39], the primitive reciprocal lattice vector of the 6×6 reconstruction $\vec{G}_{\text{SiC}}(6 \times 6)$ is very similar to the moiré vector \vec{G}'_m . Therefore, the $\varepsilon_1 - \varepsilon_6$ replicas can be explained by the 6×6 reconstruction by shifting the original Dirac cone at the K point with $\vec{G}_{\text{SiC}}(6 \times 6)$. However, the new observed Dirac cone replicas $\alpha - \delta$ are not consistent with the 6×6 reconstruction scenario. Along the $\Gamma - K$ direction, the 6×6 reconstruction would induce a series of replicas with a constant interval of $\vec{G}_{\text{SiC}}(6 \times 6)$, which disagrees with the experimental results shown in Fig. 2(b). Furthermore, as seen from Fig. 2(h), the α and β replicas show a different orientation to the

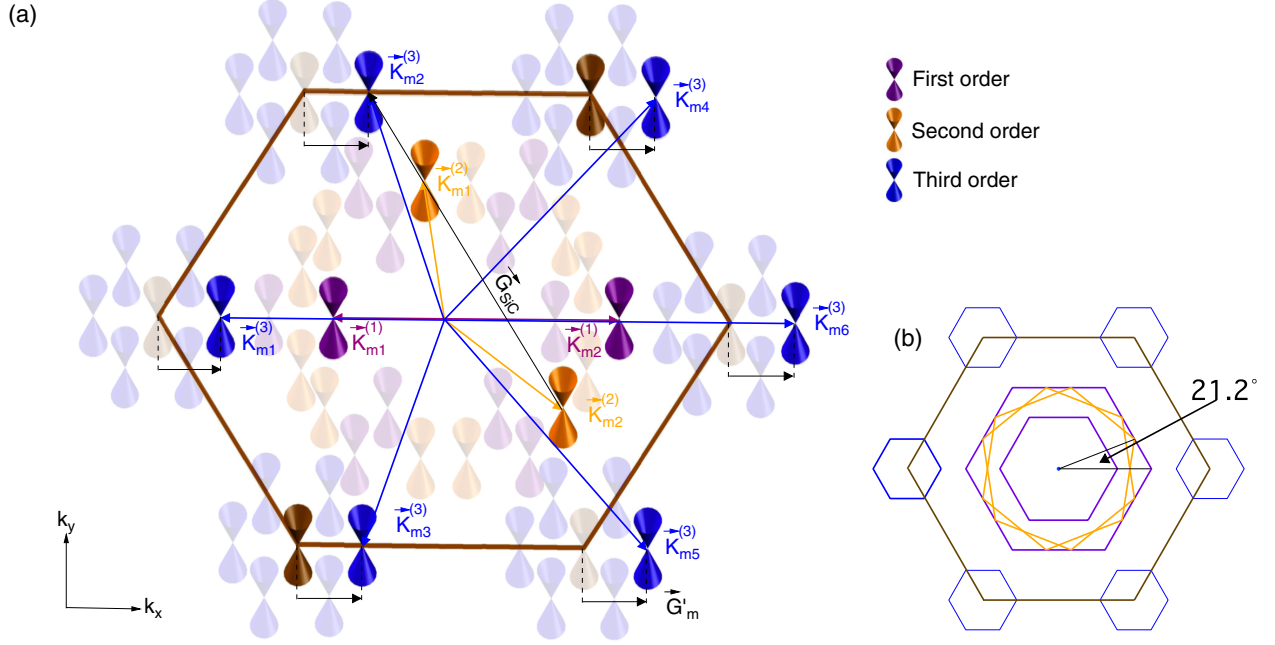


FIG. 4. (a) Schematic drawing of Dirac cone replicas induced by the high-order moiré effect in the graphene-SiC heterostructure. The first-, second-, and third-order momentum transfer vectors and corresponding Dirac cone replicas are labeled. (b) Same as (a), with the corners of hexagons indicating the Dirac cone replicas.

original Dirac cone. This behavior also cannot be explained by the 6×6 reconstruction scenario. Similarly, the $6\sqrt{3} \times 6\sqrt{3}$ reconstruction is not consistent with the new observation of Dirac cone replicas $\alpha-\delta$. The high-order moiré-effect-induced replicas without a fixed interval in the k space in graphene-SiC are also distinct from the ones in the metal monolayer on substrates, which have a constant interval [46,47].

The high-order moiré effect breaks the limitation of small lattice constant mismatch Δa for realizations of the moiré effect (more discussions in Fig. S4 in the Supplemental Material [39]). It provides an opportunity for using materials without a good lattice match but which host properties such as magnetism and superconductivity to design a moiré pattern potential and control the electronic structure. The interplays between the high-order moiré effect, quantum phases, and phase transitions deserve further investigations.

IV. CONCLUSIONS

In summary, we demonstrated the high-order moiré effect in a graphene-SiC heterostructure, defined by a'_m in real space related to a small lattice mismatch $\Delta a' = (\sqrt{3}a_{\text{SiC}} - 2a_{\text{Gra}})$ and a twist angle $\theta' = 0^\circ$ between the supercells [Fig. 1(c)] and moiré vector \vec{G}'_m in k space [Fig. 1(d)]. The high-order moiré effect on the electronic modulation in real space is clearly revealed by STM measurements and corresponding FFT results, with $a'_m = 1.9$ nm and $\vec{G}'_m = 0.38 \text{ \AA}^{-1}$. Our ARPES results uncover the high-order moiré effect in k space with the observation of multiple Dirac cone replicas $\alpha-\delta$ which cannot be explained by the reconstruction scenarios [43–45]. Figure 4 summarizes the positions of replicas with the series of momentum transfer vectors $\vec{K}_{mi}^{(n)}$ and the

geometry relationships. Like the first-order moiré effect in the graphene-BN system [40], six replicas form a hexagon centered at the K point with a distance of the moiré vector \vec{G}'_m in the graphene-SiC heterostructure [blue cones in Fig. 4(a) and blue hexagon in Fig. 4(b)]. However, such a hexagon is induced by the third-order momentum transfer in the graphene-SiC system, instead of the first-order momentum transfer in the graphene-BN system. The first- and second-order momentum transfers in the graphene-SiC system generate replicas forming a hexagon centered at the Γ point with the orientations rotated 0° and $\pm 21.2^\circ$ from the BZ of graphene, respectively. The Hofstadter butterfly states induced by the multiple Dirac cone replicas are expected under magnetic field and require further experimental investigations. Our results not only reveal a type of high-order moiré effect which could dominate heterostructures with large lattice mismatches and rotation angles but also provide a way to design the moiré effect using materials hosting properties without the limitation of good lattice constant match.

ACKNOWLEDGMENTS

We thank Shengjun Yuan and Fengcheng Wu for useful discussions. This paper was supported by the Chinese National Key Research and Development Program (Grant No. 2018FYA0305800), the Ministry of Science and Technology of China (Grant No. 2018YFA0307000), the National Natural Science Foundation of China (Grants No. U2032128, No. 11874047, and No. 11774268), the Fundamental Research Funds for the Central Universities (Grant No. 2042021kf0210), and the Strategic Priority Research Program of the Chinese Academy of Sciences (No. XDB30000000).

- [1] A. K. Geim and I. V. Grigorieva, Van der Waals heterostructures, *Nature (London)* **499**, 419 (2013).
- [2] L. A. Ponomarenko, R. V. Gorbachev, G. L. Yu, D. C. Elias, R. Jalil, A. A. Patel, A. Mishchenko, A. S. Mayorov, C. R. Woods, J. R. Wallbank, M. Mucha-Kruczynski, B. A. Piot, M. Potemski, I. V. Grigorieva, K. S. Novoselov, F. Guinea, V. I. Fal'ko, and A. K. Geim, Cloning of Dirac fermions in graphene superlattices, *Nature (London)* **497**, 594 (2013).
- [3] C. R. Dean, L. Wang, P. Maher, C. Forsythe, F. Ghahari, Y. Gao, J. Katoch, M. Ishigami, P. Moon, M. Koshino, T. Taniguchi, K. Watanabe, K. L. Shepard, J. Hone, and P. Kim, Hofstadter's butterfly and the fractal quantum Hall effect in Moiré superlattices, *Nature (London)* **497**, 598 (2013).
- [4] B. Hunt, J. D. Sanchez-Yamagishi, A. F. Young, M. Yankowitz, B. J. LeRoy, K. Watanabe, T. Taniguchi, P. Moon, M. Koshino, P. Jarillo-Herrero, and R. C. Ashoori, Massive Dirac fermions and Hofstadter butterfly in a van der Waals heterostructure, *Science* **340**, 1427 (2013).
- [5] W. Yang, G. R. Chen, Z. W. Shi, C. C. Liu, L. C. Zhang, G. B. Xie, M. Cheng, D. M. Wang, R. Yang, D. X. Shi, K. Watanabe, T. Taniguchi, Y. G. Yao, Y. B. Zhang, and G. Y. Zhang, Epitaxial growth of single-domain graphene on hexagonal boron nitride, *Nat. Mater.* **12**, 792 (2013).
- [6] G. L. Yu, R. V. Gorbachev, J. S. Tu, A. V. Kretinin, Y. Gao, R. Jalil, F. Withers, L. A. Ponomarenko, B. A. Piot, M. Potemski, D. C. Elias, X. Chen, K. Watanabe, T. Taniguchi, I. V. Grigorieva, K. S. Novoselov, V. I. Fal'ko, A. K. Geim, and A. Mishchenko, Hierarchy of Hofstadter states and replica quantum Hall ferromagnetism in graphene superlattices, *Nat. Phys.* **10**, 525 (2014).
- [7] E. Wang, X. B. Lu, S. J. Ding, W. Yao, M. Z. Yan, G. L. Wan, K. Deng, S. P. Wang, G. R. Chen, L. G. Ma, J. Jung, A. V. Fedorov, Y. B. Zhang, G. Y. Zhang, and S. Y. Zhou, Gaps induced by inversion symmetry breaking and second-generation Dirac cones in graphene/hexagonal boron nitride, *Nat. Phys.* **12**, 1111 (2016).
- [8] Y. Cao, V. Fatemi, A. Demir, S. A. Fang, S. L. Tomarken, J. Y. Luo, J. D. Sanchez-Yamagishi, K. Watanabe, T. Taniguchi, E. Kaxiras, R. C. Ashoori, and P. Jarillo-Herrero, Correlated insulator behaviour at half-filling in magic-angle graphene superlattices, *Nature (London)* **556**, 80 (2018).
- [9] Y. Cao, V. Fatemi, S. A. Fang, K. Watanabe, T. Taniguchi, E. Kaxiras, and P. Jarillo-Herrero, Unconventional superconductivity in magic-angle graphene superlattices, *Nature (London)* **556**, 43 (2018).
- [10] M. Yankowitz, S. W. Chen, H. Polshyn, Y. X. Zhang, K. Watanabe, T. Taniguchi, D. Graf, A. F. Young, and C. R. Dean, Tuning superconductivity in twisted bilayer graphene, *Science* **363**, 1059 (2019).
- [11] X. B. Lu, P. Stepanov, W. Yang, M. Xie, M. A. Aamir, I. Das, C. Urgell, K. Watanabe, T. Taniguchi, G. Y. Zhang, A. Bachtold, A. H. MacDonald, and D. K. Efetov, Superconductors, orbital magnets and correlated states in magic-angle bilayer graphene, *Nature (London)* **574**, 653 (2019).
- [12] E. Codecido, Q. Y. Wang, R. Koester, S. Che, H. D. Tian, R. Lv, S. Tran, K. Watanabe, T. Taniguchi, F. Zhang, M. Bockrath, and C. N. Lau, Correlated insulating and superconducting states in twisted bilayer graphene below the magic angle, *Sci. Adv.* **5**, eaaw9770 (2019).
- [13] A. Kerelsky, L. J. McGilly, D. M. Kennes, L. J. McGilly, L. Xian, M. Yankowitz, S. W. Chen, K. Watanabe, T. Taniguchi, J. Hone, C. Dean, A. Rubio, and A. N. Pasupathy, Maximized electron interactions at the magic angle in twisted bilayer graphene, *Nature (London)* **572**, 95 (2019).
- [14] Y. Saito, J. Y. Ge, K. Watanabe, T. Taniguchi, and A. F. Young, Independent superconductors and correlated insulators in twisted bilayer graphene, *Nat. Phys.* **16**, 926 (2020).
- [15] G. W. Burg, J. H. Zhu, T. Taniguchi, K. Watanabe, and A. H. MacDonald, Correlated Insulating States in Twisted Double Bilayer Graphene, *Phys. Rev. Lett.* **123**, 197702 (2019).
- [16] C. Shen, Y. B. Chu, Q. S. Wu, L. Na, S. P. Wang, Y. C. Zhao, J. Tang, J. Y. Liu, J. P. Tian, K. Watanabe, T. Taniguchi, R. Yang, Z. Y. Meng, D. X. Shi, O. V. Yazyev, and G. Y. Zhang, Correlated states in twisted double bilayer graphene, *Nat. Phys.* **16**, 520 (2020).
- [17] K. P. Nuckolls, M. Oh, D. Wong, B. Lian, K. Watanabe, T. Taniguchi, B. A. Bernevig, and A. Yazdani, Strongly correlated Chern insulators in magic-angle twisted bilayer graphene, *Nature (London)* **588**, 610 (2020).
- [18] Y. Cao, D. Rodan-Legrain, O. Rubies-Bigorda, J. M. Park, K. Watanabe, T. Taniguchi, and P. Jarillo-Herrero, Tunable correlated states and spin-polarized phases in twisted bilayer-bilayer graphene, *Nature (London)* **583**, 215 (2020).
- [19] X. M. Liu, Z. Y. Hao, E. Khalaf, J. Y. Lee, Y. Ronen, H. Yoo, D. H. Najafabadi, K. Watanabe, T. Taniguchi, A. Vishwanath, and P. Kim, Tunable spin-polarized correlated states in twisted double bilayer graphene, *Nature (London)* **583**, 221 (2020).
- [20] M. H. He, Y. H. Li, J. Q. Cai, Y. Liu, K. Watanabe, T. Taniguchi, X. D. Xu, and M. Yankowitz, Symmetry breaking in twisted double bilayer graphene, *Nat. Phys.* **17**, 26 (2021).
- [21] Y. Choi, H. Kim, Y. Peng, A. Thomson, C. Lewandowski, R. Polski, Y. Zhang, H. S. Arora, K. Watanabe, T. Taniguchi, J. Alicea, and S. Nadj-Perge, Correlation-driven topological phases in magic angle twisted bilayer graphene, *Nature (London)* **589**, 536 (2021).
- [22] J. M. Park, Y. Cao, K. Watanabe, T. Taniguchi, and P. Jarillo-Herrero, Tunable strongly coupled superconductivity in magic-angle twisted trilayer graphene, *Nature (London)* **590**, 249 (2021).
- [23] Z. Y. Hao, A. M. Zimmerman, P. Ledwith, E. Khalaf, D. H. Najafabadi, K. Watanabe, T. Taniguchi, A. Vishwanath, and P. Kim, Electric field-tunable superconductivity in alternating-twist magic-angle trilayer graphene, *Science* **12**, 371 (2021).
- [24] L. Balents, C. R. Dean, D. K. Efetov, and A. F. Young, Superconductivity and strong correlations in Moiré flat bands, *Nat. Phys.* **16**, 725 (2020).
- [25] P. Stepanov, I. Das, X. B. Lu, A. Fahimniya, K. Watanabe, T. Taniguchi, F. H. L. Koppens, J. Lischner, L. Levitov, and D. K. Efetov, Untying the insulating and superconducting orders in magic-angle graphene, *Nature (London)* **583**, 375 (2020).
- [26] M. Yankowitz, Q. Ma, P. Jarillo-Herrero, and B. J. LeRoy, van der Waals heterostructures combining graphene and hexagonal boron nitride, *Nat. Rev. Phys.* **1**, 112 (2019).
- [27] H. S. Arora, R. Polski, Y. R. Zhang, A. Thomson, Y. Choi, H. Kim, Z. Lin, I. Z. Wilson, X. D. Xu, J. H. Chu, K. Watanabe, T. Taniguchi, J. Alicea, and S. Nadj-Perge, Superconductivity in metallic twisted bilayer graphene stabilized by WSe₂, *Nature (London)* **583**, 379 (2020).

- [28] A. L. Sharpe, E. J. Fox, A. W. Barnard, J. Finney, K. Watanabe, T. Taniguchi, M. A. Kastner, and D. Goldhaber-Gordon, Emergent ferromagnetism near three-quarters filling in twisted bilayer graphene, *Science* **365**, 605 (2019).
- [29] M. Serlin, C. L. Tschirhart, H. Polshyn, Y. Zhang, J. Zhu, K. Watanabe, T. Taniguchi, L. Balents, and A. F. Young, Intrinsic quantized anomalous Hall effect in a Moiré heterostructure, *Science* **367**, 900 (2020).
- [30] G. R. Chen, L. L. Jiang, S. Wu, B. Lyu, H. Y. Li, B. L. Chittari, K. Watanabe, T. Taniguchi, Z. W. Shi, J. Jung, Y. B. Zhang, and F. Wang, Evidence of a gate-tunable Mott insulator in a trilayer graphene Moiré superlattice, *Nat. Phys.* **15**, 237 (2019).
- [31] G. R. Chen, A. L. Sharpe, P. Gallagher, I. T. Rosen, E. J. Fox, L. L. Jiang, B. Lyu, H. Y. Li, K. Watanabe, T. Taniguchi, J. Jung, Z. W. Shi, D. Goldhaber-Gordon, Y. B. Zhang, and F. Wang, Signatures of tunable superconductivity in a trilayer graphene Moiré superlattice, *Nature (London)* **572**, 215 (2019).
- [32] B. L. Chittari, G. R. Chen, Y. B. Zhang, F. Wang, and J. Jung, Gate-Tunable Topological Flat Bands in Trilayer Graphene Boron-Nitride Moiré Superlattices, *Phys. Rev. Lett.* **122**, 016401 (2019).
- [33] G. R. Chen, A. L. Sharpe, E. J. Fox, Y. H. Zhang, S. X. Wang, L. L. Jiang, B. Lyu, H. Y. Li, K. Watanabe, T. Taniguchi, Z. W. Shi, T. Senthil, D. Goldhaber-Gordon, Y. B. Zhang, and F. Wang, Tunable correlated Chern insulator and ferromagnetism in a Moiré superlattice, *Nature (London)* **579**, 56 (2020).
- [34] C. Repellin, Z. H. Dong, Ya-Hui Zhang, and T. Senthil, Ferromagnetism in Narrow Bands of Moiré Superlattices, *Phys. Rev. Lett.* **124**, 187601 (2020).
- [35] H. Polshyn, J. Zhu, M. A. Kumar, Y. Zhang, F. Yang, C. L. Tschirhart, M. Serlin, K. Watanabe, T. Taniguchi, A. H. MacDonald, and A. F. Young, Electrical switching of magnetic order in an orbital Chern insulator, *Nature (London)* **588**, 66 (2020).
- [36] J. T. Shi, J. H. Zhu, and A. H. MacDonald, Moiré commensurability and the quantum anomalous Hall effect in twisted bilayer graphene on hexagonal boron nitride, *Phys. Rev. B* **103**, 075122 (2021).
- [37] C. D. Zhang, C. P. Chuu, X. B. Ren, M. Y. Li, L. J. Li, C. H. Jin, M. Y. Chou, and C. K. Shih, Interlayer couplings, Moiré patterns, and 2D electronic superlattices in MoS₂/WSe₂ hetero-bilayers, *Sci. Adv.* **3**, e1601459 (2017).
- [38] Q. Y. Wang, W. H. Zhang, L. L. Wang, K. He, X. C. Ma, and Q. K. Xue, Large-scale uniform bilayer graphene prepared by vacuum graphitization of 6H-SiC (0001) substrates, *J. Phys.: Condens. Matter* **25**, 095002 (2013).
- [39] See Supplemental Material at <http://link.aps.org/supplemental/10.1103/PhysRevB.104.235130> for Supplemental Figs. S1–S4.
- [40] S. Y. Zhou, G. H. Gweon, A. V. Fedorov, P. N. First, W. A. de Heer, D. H. Lee, F. Guinea, A. H. Castro Neto, and A. Lanzara, Substrate-induced bandgap opening in epitaxial graphene, *Nat. Mater.* **6**, 770 (2007).
- [41] S. J. Ahn, P. Moon, T.-H. Kim, H.-W. Kim, H.-C. Shin, E. H. Kim, H. W. Cha, S.-J. Kahng, P. Kim, M. Koshino, Y.-W. Son, C.-W. Yang, and J. R. Ahn, Dirac electrons in a dodecagonal graphene quasicrystal, *Science* **361**, 782 (2018).
- [42] Y. Wei, E. Wang, C. H. Bao, Y. O. Zhang, K. N. Zhang, K. J. Bao, C. K. Chan, C. Y. Chen, J. Avila, M. C. Asensio, J. Y. Zhu, and S. Y. Zhou, Quasicrystalline 30° twisted bilayer graphene as an incommensurate superlattice with strong interlayer coupling, *Proc. Natl Acad. Sci.* **115**, 6928 (2018).
- [43] P. Lauffer, K. V. Emtsev, R. Graupner, Th. Seyller, L. Ley, S. A. Reshanov, and H. B. Weber, Atomic and electronic structure of few-layer graphene on SiC (0001) studied with scanning tunneling microscopy and spectroscopy, *Phys. Rev. B* **77**, 155426 (2008).
- [44] E. Rollings, G. H. Gweon, S. Y. Zhou, B. S. Mun, J. L. McChesney, B. S. Hussain, A. Fedorov, P. N. First, W. A. de Heer, and A. Lanzara, Synthesis and characterization of atomically thin graphite films on a silicon carbide substrate, *J. Phys. Chem. Solids* **67**, 2172 (2006).
- [45] C. Berger, Z. M. Song, T. B. Li, X. B. Li, A. Y. Ogbazghi, R. Feng, Z. T. Dai, W. A. N. Marchenkov, E. H. Conrad, P. N. First, and W. A. de Heer, Ultrathin epitaxial graphite: 2D electron gas properties and a route toward graphene-based nanoelectronics, *J. Phys. Chem. B* **108**, 19912 (2004).
- [46] J. N. Crain, K. N. Altmann, C. Bromberger, and F. J. Himpsel, Fermi surfaces of surface states on Si(111)-Ag, Au, *Phys. Rev. B* **66**, 205302 (2002).
- [47] E. Rotenberg, H. Koh, K. Rossnagel, H. W. Yeom, J. Schäfer, B. Kernzer, M. P. Rocha, and S. D. Kevan, Indium 7 × 3 on Si(111): A Nearly Free Electron Metal in Two Dimensions, *Phys. Rev. Lett.* **91**, 246404 (2003).